Finite Element Studies on Friction Stir Welding Processes of Polyethylene Plates

M. Naseri[1], Mohammad Alipour[2], A. Ghasemi[3,*] and E. Davari[4]

* *a.ghasemi@iau-tnb.ac.ir*

Received: December 2017 Accepted: February 2018

[1] Department of Materials Science and Engineering, Faculty of Engineering, Shahid Chamran University of Ahvaz, Ahvaz, Iran.

[2] Department of Materials Science and Engineering, University of Tabriz, Tabriz, Iran.

[3] Department of Mechanical Engineering, Faculty of Engineering, North Tehran Branch, Islamic Azad University, Tehran, Iran.

[4] Department of Chemistry, Tarbiat Modares University, Tehran, Iran.

DOI: 10.22068/ijmse.15.1.40

Abstract: *One of the interesting state-of-the-art approaches to welding is the process of friction stir welding (FSW). In comparison with the fusion processes, FSW is an advantageous method as it is suitable for the non-fusion weldable alloys and polymeric materials joining. Regarding the materials pure solid state joining, it also provides joints with less distortion and enhanced mechanical properties. In the present work, a three-dimensional (3D) model based on finite element analysis was applied to study the thermal history and thermomechanical procedure in friction stir welding of high density polyethylene plate. The technique includes the tool mechanical reaction and the weld material thermomechanical procedure. The considered heat source in the model, includes the friction among three items: the material, the probe and the shoulder. Finally, the model was validated by measuring actual temperatures near the weld nugget using thermocouples, and good agreement was obtained for studied materials and conditions.*

Keywords: *Polyethylene (PE); Friction stir welding (FSW); Finite element method (FEM); Temperature distribution; Thermomechanical model.*

[Downloaded from idea.iust.ac.ir on 2024-07-29]

[DOI: 10.22068/ijmse.15.1.40]

1. INTRODUCTION

Polyethylene (PE) has been consumed in vast applications. For instance, polymer films, containers made of polymer, pipes, and toys are the known productions. The PE notable advantages over materials with traditional structures can be mentioned as the light weight decreasing the expenses in transportation and installation, omission of the rust and therefore reduce problems in some sensitive industries [1-3]. Consuming polyethylene in pipe and other structural usages are prevalent on account of the aforementioned causes. Moreover, in the complicated loading conditions in industry, joints between polymeric structures are inevitable. Accordingly, desired light weight and the advanced performance are obtained through this novel welding method [4, 5]. Based on heat generation technic, polymers can be welded via three methods: (i) methods employing an external heat source, (ii) methods where heat is generated by mechanical movement and (iii) methods which directly employ electromagnetism [6].

Friction stir welding (FSW) is a solid state, i.e. without melting in the workpiece, joining technique that is intended to be used for joining of especially the aluminum alloys, besides dissimilar welds, which are difficult to weld with traditional welding techniques [7, 8]. Joining of large panels, which cannot be easily heat treated post weld to recover temper characteristics, is another common interest for FSW to be preferred for industrial applications besides its other benefits. Through FSW, a cylindrical-shouldered structure, including a probe (pin), which can be designed cylindrical/profiled or threaded/ unthreaded, rotates with a constant pace and moves at a constant traverse speed along with the joint line of two sheet pieces or plates, operating the welding process, Fig.1. As there are great applied plunging forces from the machine head while FSW, the parts must be fixed firmly onto a backing plate, so that they won't become disrupted [9, 10]. Compared to the desired weld depth, the pin length is a little less, and the

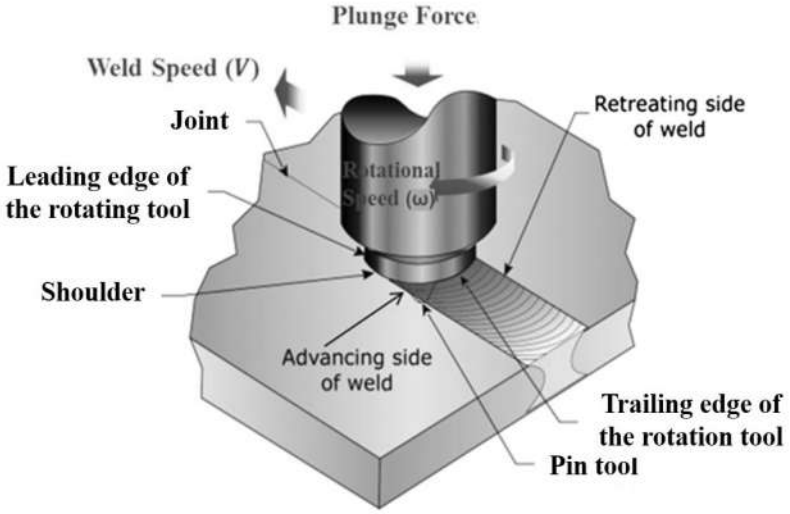

Fig. 1. Schematic of friction stir welding (FSW) process.

shoulder device should be in contact with the workpiece, directly. The probe is submerged into the workpiece and then the tool is moved along the weld line with a tilt angle of 2-4 degress increasing the pressure under the tool shoulder. During this solid state welding process, problems such as liquation cracking, porosity, and distortion that take place during conventional welding methods do not occur. Furthermore, the process does not involve any use of filler metal and therefore, in contrast to fusion welding, the compatibility of composition is not an issue in FSW [11-13].

Though the FSW technique was mainly innovated for the alloys of aluminum, it is also capable approach to welding of various types of material like copper [14, 15], steel [9], magnesium [16, 17], titanium [18], and other combinations [19-21]. Recently, some researchers have studied the application of FSW and to thermoplastic materials [22-26]. The thermomechanical conditions and the material flow while friction stir welding of polymers, have been investigated through a research by Simoes and Rodrigues [24]. According to their survey, considering the rheological and physical properties of polymers, FSW thermomechanical conditions of polymers totally differ from defined conditions for metals. So, quiet different material flow mechanisms and the weld defect morphologies are obtained. Possibility of friction spot welding (FSpW) of a commercial poly (methyl methacrylate) (PMMA) GS grade and a PMMA 6 N/2 wt% silica (SiO_2) nanocomposite were investigated by Junior et al. [27] researched. With this study, it was revealed that the joint produced at 1000 rpm shows sharp weld lines, demonstrating insufficient heat input. In addition, in the welded area, weld productions prepared at 3000 rpm seem to have further plastic deformation, more volumetric defects, and a lack of material mixing, reckoning the higher heat input. Bozkurt [25] research has been conducted on the feasibility of the FSW carried out on high density polyethylene (HDPE) sheets, utilizing the Taguchi technique. By this study, tool rotation rate notable impact was clarified and determined as 73.85% of the total welding parameters (including traverse speed and tilt angle). Defined optimum welding parameters for the ultimate tensile strength are as follows; the tool rotation speed of 3000 rpm, the tool traverse speed of 115 mm/min, and the tilt angle of 3°. Recently, the effect of weld parameters such as the rotational speed, traverse speed, and geometry and tilt angle of the tool has been compared to the quality and creep properties of friction stir welded high density polyethylene plate joints studied by Hoseinlaghab et al. [27]. The experimental results showed that by increasing tool tilt angle,

[Downloaded from idea.iust.ac.ir on 2024-07-29]

[DOI: 10.22068/ijmse.15.1.40]

lower weld quality and creep resistant were achieved. Meanwhile, pins with the cylindrical geometry are preferred in comparison to pins with conical geometry.

Several analytical and numerical models are being studied by many research groups in order to improve the process efficiency and performance of the components [28]. Various aspects of modeling FSW are possible regarding microstructure evolution, material and heat flow, heat generation, investigation of the influence of process parameters, residual stress computation, predicting mechanical loads (tool forces, torque, and adjustment of work piece fixture, etc.) and final mechanical properties of the joint [29-31]. Thermal models are of great interest because they are often used as input for modeling some of the aspects mentioned above. Although analytical models cannot substitute the state-of-the-art numerical models, they introduce a substantial flexibility and effectiveness in industrial design applications, and moreover they also contribute strongly to increasing the basic understanding of the process [28, 32]. Through current investigation, based on a finite element method (FEM), a three-dimensional (3D) model has been suggested to evaluate the thermal effect in the weld. Here, through parametrical study, it has been revealed that how various welding factors, the tool rotation rate and the tool traverse speed, influence results. The welding procedure is entirely simulated by the commercial finite element package ANSYS 14. Experiments on a welding of polyethylene plates are also carried out. Also, the temperature history for the welded plates are measured by the Labview-programmed acquisition system.

2. MODEL DESCRIPTION

Joining polyethylene by FSW has been a great interest for research nowadays [23, 25, 27, 33, 34]. The simulation of FSW process on the specimens was carried out through the finite element model. On account of having desired ductility, capable for elastic, plastic, large strain, large deformations and isotropic hardening effect simulation, a rigid solid tool and a workpiece were basis of the model. A 3D 20-node coupled-field solid element was taken up in order to model the workpiece and tool in ANSYS® 14. According to the FSW speed evaluations brought

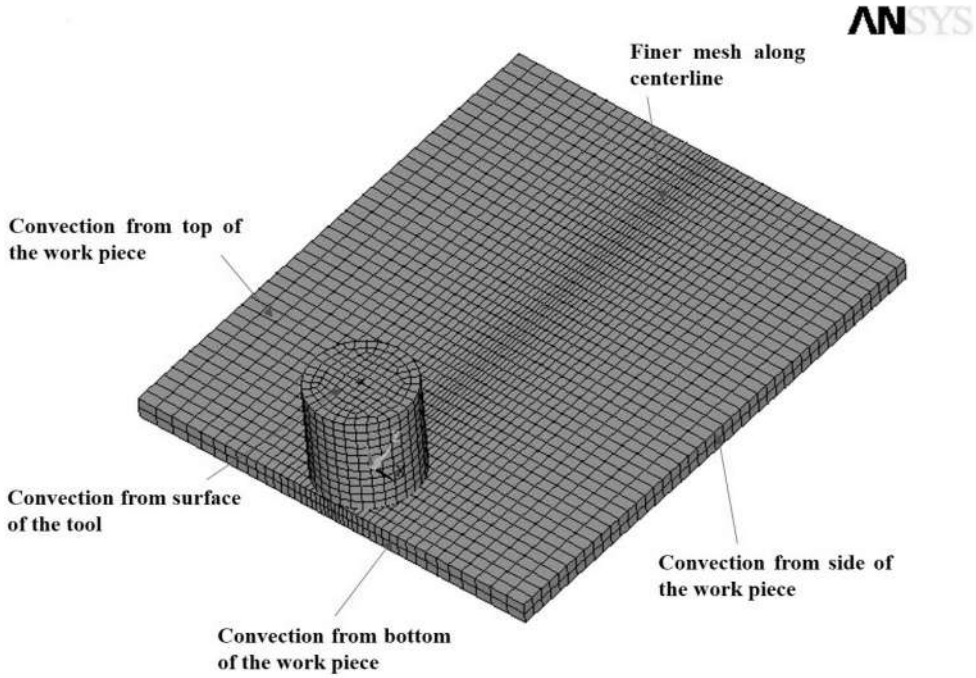

Fig. 2. Meshes and thermal boundary conditions of the finite element model.

[Downloaded from idea.iust.ac.ir on 2024-07-29]

[DOI: 10.22068/ijmse.15.1.40]

in this research, elastic and plastic behavior of the plate was presumed independent of the rate [36]. The illustration of a meshed welded plate with the total nodes of 12649 (Fig. 2), is indicating the symmetry along the weld line considering the numerical evaluation.

2. 1. Material and Associated Flow Model

The FSW model presented in this paper used a rate-independent plasticity material, where three distinct criteria have been used to determine rate-independent plasticity model and these are: (i) flow rule, (ii) hardening rule and (iii) yield criterion. Flow rule determines the increment in plastic strain from the increment in load. In the current analysis, associative flow rule is used, which is represented by Eq. (1):

$$\{d\varepsilon^{p1}\} = d\lambda\left\{\frac{\partial G}{\partial \sigma}\right\} \tag{1}$$

where $d\varepsilon^{p1}$ is the change in plastic strain, $d\lambda$ is the magnitude of the plastic strain increment, G is the plastic potential (which determines the direction of plastic straining) and $\partial\sigma$ is the change in stress. The von Mises yield criterion has been applied in the current analysis as a yield criterion. The von Mises yield criterion is represented by Eqs. (2) and (3) [36]:

$$f(\sigma,\sigma_y) = \sigma_e - \sigma_y = 0 \tag{2}$$

$$\sigma_e = \sqrt{\frac{3}{2}\left(\sigma:\sigma - \frac{1}{3}tr(\sigma)^2\right)} \tag{3}$$

where σ_e is the von Mises effective stress, σ_y is the yield strength and tr is the Tresca criterion. The total amount of plastic work is the sum of the plastic work done over the history of loading as expressed by Eq. (4):

$$\chi = \int \{\sigma\}^T [M]\{d\varepsilon^{p1}\} \tag{4}$$

where χ is the plastic work, $[M]$ is the mass matrix and σ is the Cauchy stress tensor.

The amount of frictional work has been calculated by Eq. (5) [36];

$$R = \tau \times \gamma \tag{5}$$

where R is the frictional work, τ is the equivalent frictional stress and is the sliding rate.

2. 2. Contact Condition

The critical part in numerical modeling of FSW is simulating the contact condition between various parts, i.e., workpiece, pin tool, and shoulder. In this research, modified Coulomb's law is applied to describe the friction force between the tool and the workpiece. During sticking condition, the matrix close to the tool surface sticks to it. Shearing is considered to address the velocity difference between the layer of the stationary material points and the material moving with the tool. The shear yield stress, τ_{yield}, is taken as:

$$\tau_{yield} = \frac{\sigma_y}{\sqrt{3}} \tag{6}$$

where σ_y is the yield strength of the material. In the presented model, the contact shear stress was taken equal to the shear yield stress, which depends on the temperature:

$$\tau_{contact} = \tau_{yield} = \frac{\sigma_y}{\sqrt{3}} \tag{7}$$

During sliding condition, the tool surface and the workpiece material slide with respect to each other. Using Coulomb's friction law, the shear stress necessary for sliding is:

$$\tau_{contact} = \tau_{yield} = \mu p = \mu\sigma \tag{8}$$

where p is the contact normal pressure, μ is the friction coefficient and σ is the contact stress. In the current analysis, according to the modified Coulomb's model, when the contact shear stress, $\tau_{contact}$, is less than the maximum frictional stress, $\tau_{\max}$, a sticking condition is modeled. Conversely, when the contact shear stress, $\tau_{contact}$, exceeds $\tau_{\max}$, the contact and the target surface will slide relative to each other, (i.e., sliding

[Downloaded from idea.iust.ac.ir on 2024-07-29]

[DOI: 10.22068/ijmse.15.1.40]

condition is modeled).

2. 3. Thermal Boundary Condition

The quantity of heat input and heat output through FSW still needs to be discussed. Considerable endeavor can determine the heat portion flowing into the tool and the plates. It strongly depends on various factors like the varying friction coefficient, downward force, temperature and the tribology of the surfaces in contact. The frictional heating at the tool welding plate interface and the plastic energy dissipation owing to shear deformation in the nugget zone General, are the two origins that heat generation arises from them. Transient heat transfer process during FSW process can be described by the Eq. (1) and the ruling equation equals:

$$\rho c_p \frac{\partial T}{\partial t} = k\left(\frac{\partial^2 T}{\partial x^2} + \frac{\partial^2 T}{\partial y^2} + \frac{\partial^2 T}{\partial z^2}\right) + Q \quad (9)$$

where Q, c_p, ρ, k and T are the heat generation, specific mass heat capacity, density of the material, thermal conductivity and absolute temperature, respectively. In finite element formulation, Eq. (1) can be represented by Eq. (2):

$$C(t)\dot{T} + K(t) = Q(t) \quad (10)$$

where $C(t)$, $\dot{T}$, $K(t)$ and $Q(t)$ are the time-dependent capacitance matrix, temperature derivative with respect to time (i.e., $\frac{dT}{dt}$), time-dependent conductivity matrix and the time-dependent heat vector, respectively.

It is assumed that convection from the free surfaces, as can be seen in Fig. 2, is the main reason for heat loss in the workpiece. The heat loss from both the side and the top surfaces is calculated using Eq. (11):

$$q_1 = h_{con}\left(T - T_0\right) \quad (11)$$

where T represents the absolute temperature of the workpiece, T_0 is the ambient temperature and h_{con} is the convection coefficient. At the bottom, a backing plate is placed to oppose the downward plunge force. This backing plate also acts as a high heat sink absorbing heat rapidly during welding; consequently, a high heat transfer coefficient is used to model the heat transfer from backing plate. The heat loss from backing plate is modeled by Eq. (12):

$$q_b = h_b\left(T - T_0\right) \quad (12)$$

where h_b represents the convection heat coefficient from backing plate. Due to the complexity associated with determining contact conditions between the workpiece and the backing plate, the value of h_b was calibrated to match experimental data, which was found to be 300 W/m^2. Heat loss from tool surface was calculated using Eq. (13):

$$q_w = h_w\left(T - T_0\right) \quad (13)$$

where h_w represents the convection heat coefficient from the pin tool. A value of 30 W/m^2 has been used as heat transfer coefficient from tool surface in the present model, which is calibrated to best fit the experimental data. All other thermal boundary conditions of current analysis are shown in Fig. 2.

2. 4. Mechanical Boundary Condition

To provide thermomechanical analysis, a conversion of thermal model into a mechanical model can be performed changing the element type SOLID226 (Fig. 3) while the mesh and load step size remain the same [35]. When the thermal analysis is fully carried out, the results are recorded for the mechanical model preparation. As a result of the created thermal strain and thermal stress in the workpiece, the plates will be deformed and distorted.

In order to be in accordance with the actual welding conditions, boundary conditions have been defined in the model. For the clamped workpiece, the boundary condition was determined as total displacement restraint:

$$U = 0 \quad (14)$$

The workpiece other parts were presumed to

[Downloaded from idea.iust.ac.ir on 2024-07-29]

[DOI: 10.22068/ijmse.15.1.40]

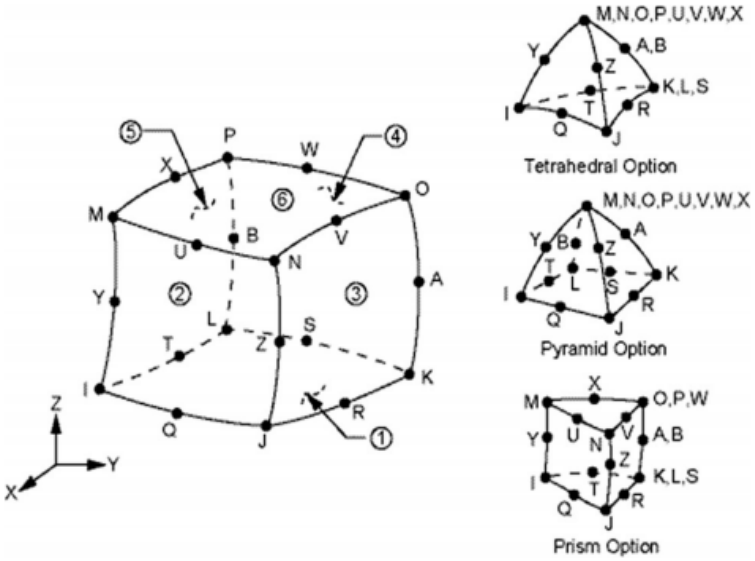

Fig. 3. Three dimensional thermal solid element SOLID226 [36].

be restrained in normal direction, where it was supported on the backing plate:

$$U_Z = 0 \tag{15}$$

3. EXPERIMENTAL PROCEDURE

High density polyethylene plate was supplied as 6.5 mm thick sheet 200 mm long and 100 mm wide, some characteristics of the material were given in Table 1. Hot worked H13 steel tool, which had 18 mm shoulder diameter, 6 mm diameter and 6 mm length in the pin was utilized. Friction stir welding had the back tilting angle of the tool 3° during its process. At two tool traverse speed of 20 mm/min and 40 mm/min there was an alteration in tool rotation rate in a range from 700 rpm to 2000 rpm. After trial and error method optimum ranges of FSW parameters were ascertained. Four thermocouples were fixed in one plate located below the top surface (the optimized range) in order to do the experiments. Thus using a Labview-programmed acquisition system, temperatures were attained and recorded in a time-duration of 0.1 s.

The microstructures of all the samples were examined by VEGA\\TSCAN field emission scanning electron microscope (FESEM). Prior to FESEM, the longitudinal sections of the samples were mechanically ground and polished to 2000-grit using SiC paper.

4. RESULTS AND DISCUSSION

4. 1. Weld Morphology Analysis

The first round to optimize friction stir welding parameters is to obtain a defect-free weld between polyethylene plates without large

Table 1. Physical and mechanical properties of HDPE [24].

Molecular weight	Density	Young's modulus	Hardness	Melting point	Thermal conductivity	Softening temperature
28.0 g	0.930–0.965 g/cm^3	1035 N/mm^2	55–70 (Shore D Scale)	135 °C	0.40–0.47 W/m K	112–130 °C

[Downloaded from idea.iust.ac.ir on 2024-07-29]

[DOI: 10.22068/ijmse.15.1.40]

cracks or grooves on the surface. For instance, in inadequate weld temperatures, regarding low rotational rates or high traverse paces, the weld material is not able to resist extensive deformation while welding. This could lead to long, tunnel-like defects on the surface or subsurface, moving along the welding. The low temperature is also a limiting factor for the tool forging and accordingly, decreases the bond continuity between the materials existing in each side of the welding. As long as the pin is not long enough or the tool comes out of the plate and also the interface at the bottom of the weld may not be disrupted and forged by the tool, the lack of penetration defect occurs [29, 37]. FSW was carried out on the structure of polyethylene at varied welding parameters to settle a suitable parameter window (Table 2). After the weld visual surfaces and cross sections examination, to continue the investigation, a satisfactory set of welding conditions was selected to produce an appropriate joint. As can be seen in Fig. 4, typical defined parameters for the process producing acceptable joints, included a translation speed of 20 mm/min and counterclockwise rotation at a rate of 1400 rpm.

Table 2. Summary of FSW parameters for polyethylene plate.

Sample no.	Rotational speed (rpm)	Traverse speed (mm/min)
1	700	20
2	1000	20
3	1400	20
4	1400	40
5	2000	20
6	2000	40

The resultant weld microstructure from the physical process dynamics is severely related to the thermal impacts history and/or plastic deformation on the weld area. Moreover, distribution of the temperature and plastic deformation are factors influencing the residual stress distribution [12, 30]. Field emission scanning electron microscopy (FESEM) of the base materials (polyethylene plates) and stir zone are shown in the Fig. 5. The grain evolution between the base material and the welded affected material is evident. A great deal of

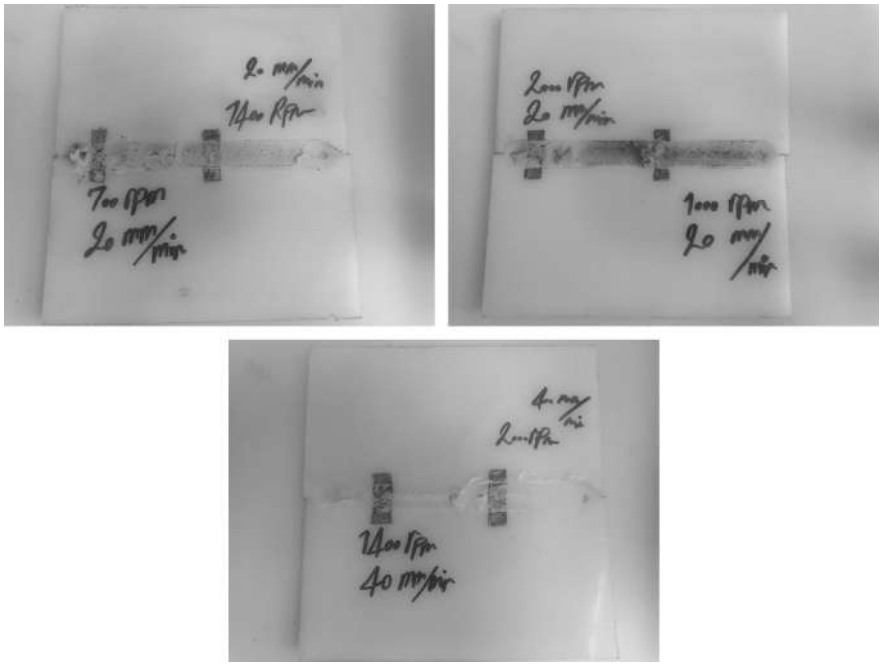

Fig. 4. Surface appearance of friction stir weld joints.

[Downloaded from idea.iust.ac.ir on 2024-07-29]

[DOI: 10.22068/ijmse.15.1.40]

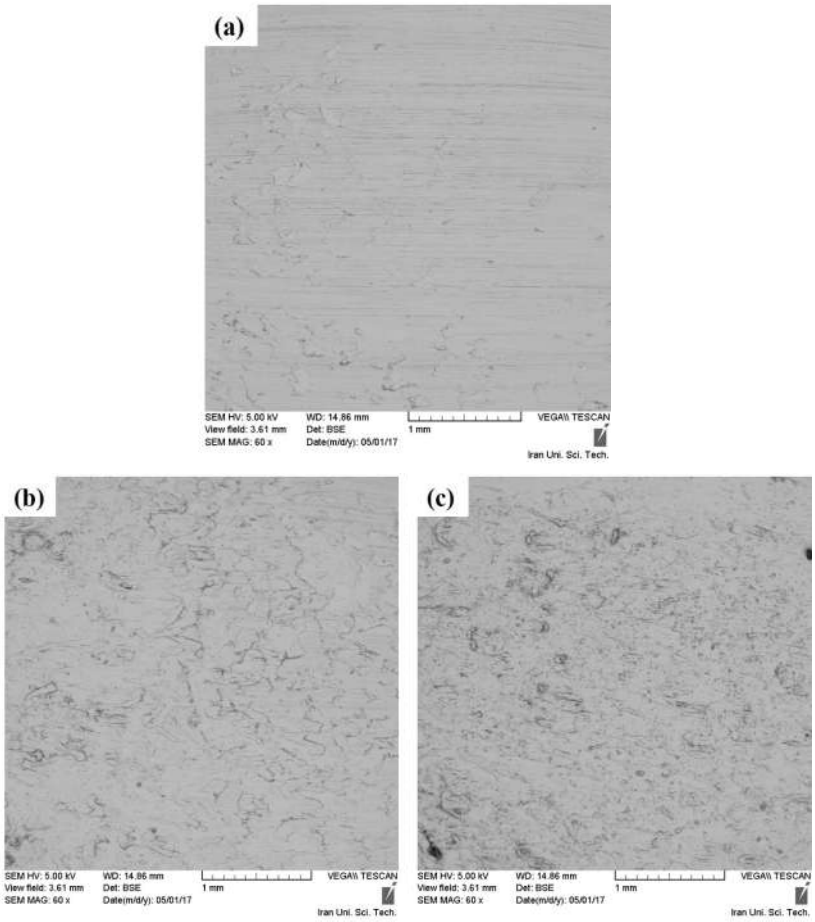

Fig. 5. Microstructures of (a) base materials and (b and c) stir zone at 1400 rpm–20 mm/min.

macro-mechanical interlocking in microstructure is formed by friction stir welding process. The fine equiaxed grains and the fragments in various dimensions at stir zone, are due to the non-uniform distribution of temperature, and the material advance and retreat flow into the sides. As the FSW is processing, the heat is localized between the tool and the workpiece. This makes the material around the pin soft. Accordingly, the tool rotation and translation can move the material in front of the leading edge, towards the pin trailing edge [11, 14, 19].

4. 2. Study of Thermal History in FSW

Figs. 6 and 7 show the temperature distribution on the top surface of the workpiece in the first, second and third load steps (1400 rpm–20 mm/min). As it can be seen, extremely high temperature gradients through the thickness of the workpieces take place below the tool shoulder area. The maximum temperature created by the FSW ranges from 80% to 90% of the melting temperature of the welding material [36, 37]. Within the stir zone, the lateral surface of shoulder to the pin root side has the highest temperature. This considerable heat flux is as a result of the shoulder rotation and the pin contacts with the plate. Furthermore, in comparison with the retreating side (RS), the advancing side (AS) experiences the greater temperature. The reason can be explained by the higher shear rates in advancing side. As in the advancing side, the tool tangential velocity is in the opposite direction with the weld velocity, the shear rates increase [21, 24, 28].

[Downloaded from idea.iust.ac.ir on 2024-07-29]

[DOI: 10.22068/ijmse.15.1.40]

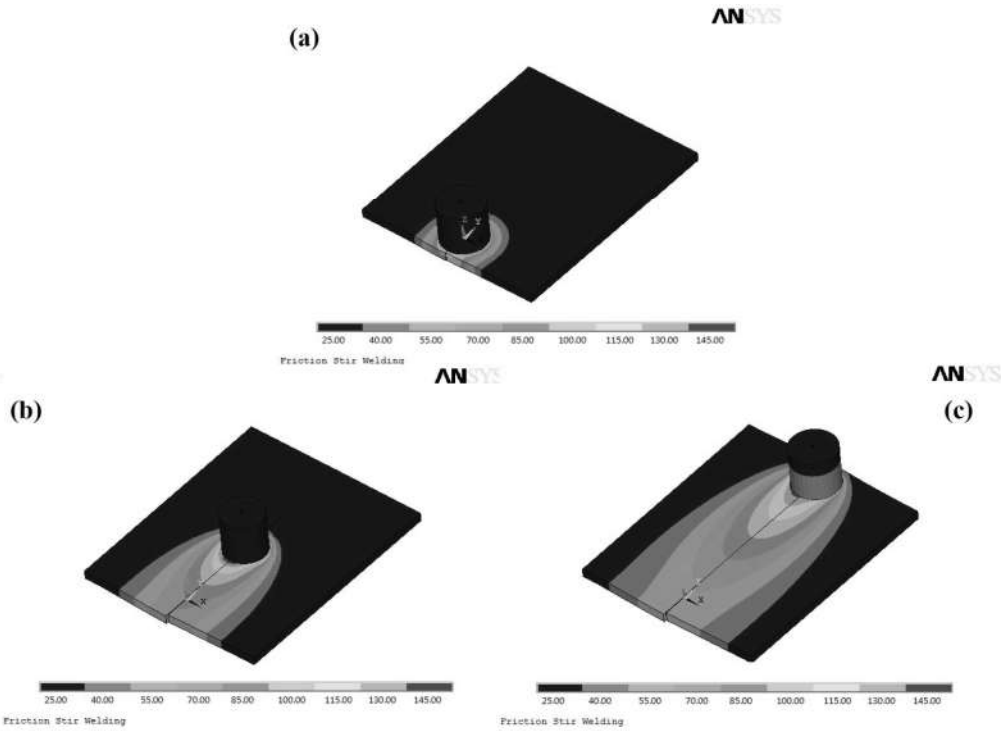

Fig. 6. Temperature map distribution at the (a) first, (b) second and (c) third load steps of the simulation (1400 rpm–20 mm/min).

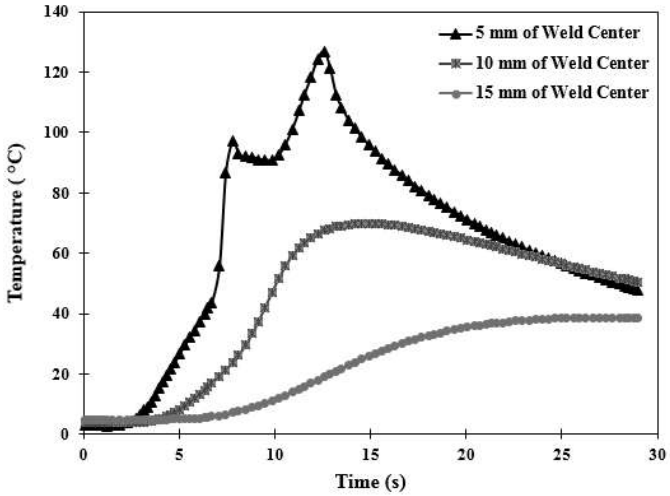

Fig. 7. Simulated top surface temperature distribution (1400 rpm–20 mm/min).

In Fig. 8, the variation in temperature with respect to time at location (5 mm to the weld center line and 0.5 mm below the upper surface of the workpiece) curves obtained from experimental results and FEM simulation are compared. At the first step of the welding process, the calculated values are greater than the measured ones and less than the obtained values when the temperature reaches maximum. Concerning assumption for the constant temperature of the backing plate while welding, the increment in the backing plate temperature is

[Downloaded from idea.iust.ac.ir on 2024-07-29]

[DOI: 10.22068/ijmse.15.1.40]

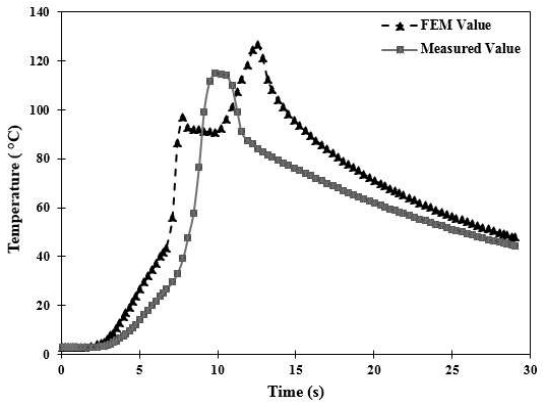

Fig. 8. A comparison of the calculated and the measured temperature histories for the location 5 mm to the weld centerline of the workpiece (1400 rpm–20 mm/min).

actually owing to the heat rise. Moreover, the cooling rate reductions at the welding final step is the other reason. The calculated values for the temperature gradient are reasonably in accordance with the measured values for the entire welding procedure.

4. 3. Analysis of Stress Distribution in the Weld

During the welding process, stress in the weld is created as a result of the material expansion while heating the welded plates and the following contraction when cooling the welds. Additionally, the weld zone mechanical reaction, regarding the tool rotational and transverse movements, affects the weld zone and increase the stress in the weld [17, 28, 36]. Fig. 9 shows the stress contours on the top surface of the workpiece in the first, second and third load steps (1400 rpm–20 mm/min). Also, Fig. 10 shows the variations of total strains of FSW processed plates. As can be seen compared with the second load step of the plate, the first and third load steps of the weld contain varied stress distributions, which may be arisen from the variance in the correlated thermomechanical process during the welding. In addition, the high temperature gradient (see Fig. 6) and high shear force by the shoulder periphery edge in this region are

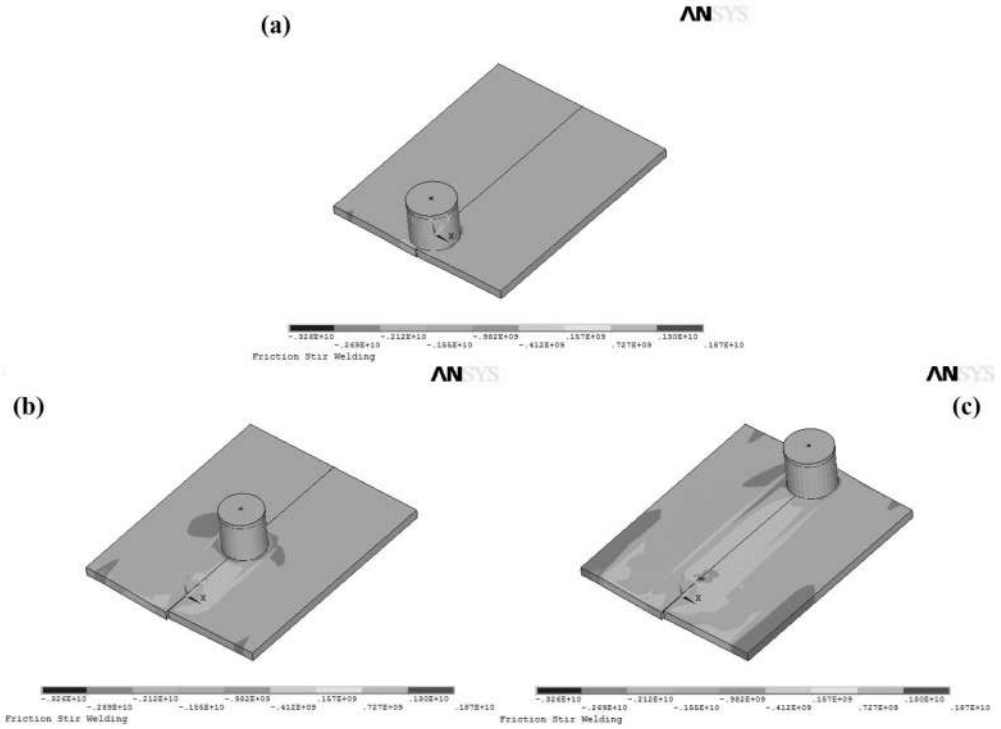

Fig. 9. Stress contours at the (a) first, (b) second and (c) third load steps of the simulation (1400 rpm–20 mm/min).

[Downloaded from idea.iust.ac.ir on 2024-07-29]

[DOI: 10.22068/ijmse.15.1.40]

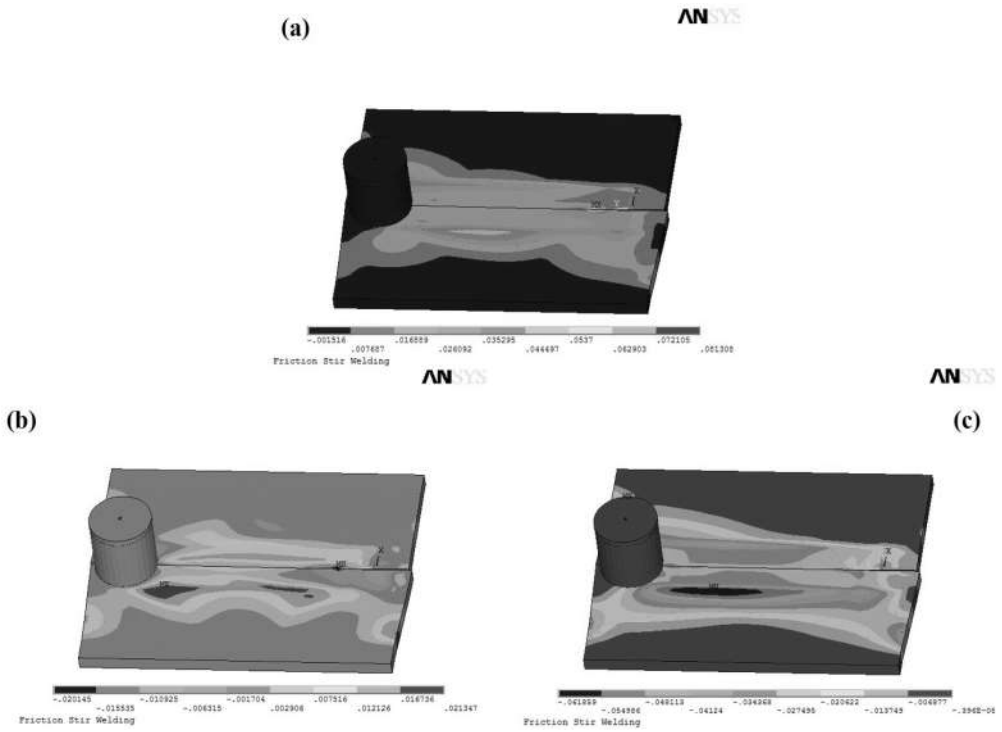

Fig. 10. Total strain contours of FSW processed polyethylene plates (a) total strain 1, (b) total strain 2 and (c) total strain 3.

considered to make the locations of the high gradient in the stresses in both the longitudinal and the lateral directions be in the closeness of the shoulder diameter.

5. CONCLUSIONS

Through this survey, the shoulder mechanical action and the thermomechanical impact of the welded material were presented as a three-dimensional (3D) model to the friction stir welding (FSW) of polymeric materials, in order to better understand the FSW thermomechanical procedure. During the FSW process performed on high density polyethylene plate, the temperature modeling and measurement, and the stress investigation have been carried out to confirm the model efficiency. The predicted values and the temperature measurements clarified that the maximum temperature gradients in longitudinal direction were on the location beyond the shoulder edge limits. The records also showed acceptable accordance with the experimentally determined temperatures.

REFERENCES

1. Ahani, M., Khatibzadeh, M. and Mohseni, M., "Studying the thermodynamic parameters of disperse dyeing of modified polyethylene terephthalate sheets using hyperbranched polymeric additive as a nanomaterial", J. Ind. Eng. Chem. 2013, 19, 1956-1962.
2. Honaker, K., Vautard, F. and Drzal, L. T., "Investigating the mechanical and barrier properties to oxygen and fuel of high density polyethylene–graphene nanoplatelet composites", Mater. Sci. Eng. B., 2017, 216, 23-30.
3. Lozano-Sánchez, L. M., Sustaita, A. O., Soto, M., Biradar, S, Ge, L., Segura-Cárdenas, E., Diabb, J., Elizalde, L. E., Barrera, E. V. and Elías-Zúñiga, A., "Mechanical and structural studies on single point incremental forming of polypropylene-MWCNTs composite sheets", J. Mater. Process. Technol. 2017, 242, 218-227.
4. Cassidy, J., Nesaei, S., McTaggart, R. and Delfanian, F., "Mechanical response of high density polyethylene to gamma radiation from a

[Downloaded from idea.iust.ac.ir on 2024-07-29]

[DOI: 10.22068/ijmse.15.1.40]

Cobalt-60 irradiator", Polym Test. 2016, 52, 111-116.
5. Liu, J. G. and Xue, W., "Formability of AA5052/polyethylene/AA5052 sandwich sheets", Trans. Nonferrous Met. Soc. China. 2013, 23, 964-969.
6. Arici, A. and Sinmazçelýk, T., "Effects of double passes of the tool on friction stir welding of polyethylene", J. Mater. Sci. 2005, 40, 3313-3316.
7. Thomas, W. M., Nicholas, E. D., Needham, J. C., Murch, M. G., Temple-Smith, P. and Dawes, C. J., "International Patent Application PCT/GB92/02203 and GB Patent Application 9125978.8", UK Patent Office, London, December 6, 1991.
8. Dawes, C. J. and Thomas W. M., TWI Bulletin 6, November/December, 1995, 124.
9. Mira-Aguiar, T, Verdera, D, Leitão, C, and Rodrigues, D. M., "Tool assisted friction welding: A FSW related technique for the linear lap welding of very thin steel plates", J. Mater. Process. Technol. 2016, 238, 73-80.
10. Sahu, P. K. and Pal, S., "Mechanical properties of dissimilar thickness aluminium alloy weld by single/double pass FSW", J. Mater. Process. Technol. 2017, 243, 442-455.
11. Kermanidis, A. T. and Tzamtzis, A., "An experimental approach for estimating the effect of heat affected zone (HAZ) microstructural gradient on fatigue crack growth rate in aluminum alloy FSW", Mater. Sci. Eng. A., 2017, 691, 110-120.
12. Sree Sabari, S., Malarvizhi, S. and Balasubramanian, V., "Characteristics of FSW and UWFSW joints of AA2519-T87 aluminium alloy: Effect of tool rotation speed", J. Manuf. Process., 2016, 22, 278-289.
13. Naseri, M., Reihanian, M. and Borhani, E., "Bonding behavior during cold roll-cladding of tri-layered Al/Brass/Al composite", J. Manuf. Process., 2016, 24, 125–137.
14. Khodaverdizadeh, H., Mahmoudi, A., Heidarzadeh, A. and Nazari, E., "Effect of friction stir welding (FSW) parameters on strain hardening behavior of pure copper joints", Mater. Des. 2012, 35, 330-334.
15. Fattah-alhosseini, A., Taheri, A. H. and Keshavarz, M. K., "Effect of friction stir welding on electrochemical behavior of pure copper", Trans. Ind. Inst. Met. 2016, 69, 1423-1434.
16. Dorbane, A., Ayoub, G., Mansoor, B., Hamade, R. F., Kridli, G., Shabadi, R. and Imad, A., "Microstructural observations and tensile fracture behavior of FSW twin roll cast AZ31 Mg sheets", Mater. Sci. Eng. A., 2016, 649, 190-200.
17. Sahu, P. K. and Pal, S., "Influence of metallic foil alloying by FSW process on mechanical properties and metallurgical characterization of AM20 Mg alloy", Mater. Sci. Eng. A., 2017, 684, 442-455.
18. Fattah-alhosseini, A, Attarzadeh, F. R. and Vakili-Azghandi, M., Effect of multi-pass friction stir processing on the electrochemical and corrosion behavior of pure titanium in strongly acidic solutions, Metall. Mater. Trans. A. 2017, 48, 403-411.
19. Khan, N. Z., Siddiquee, A. N., Khan, Z. A. and Mukhopadhyay, A. K., "Mechanical and microstructural behavior of friction stir welded similar and dissimilar sheets of AA2219 and AA7475 aluminium alloys", J. Alloys Compd. 2017, 695, 2902-2908.
20. Luo, C., Li, X., Song, D., Zhou, N., Li, Y. and Qi, W., "Microstructure evolution and mechanical properties of friction stir welded dissimilar joints of Mg–Zn–Gd and Mg–Al–Zn alloys", Mater. Sci. Eng. A., 2016, 664, 103-113.
21. Fattah-alhosseini, A., Vakili-Azghandi, M., Sheikhi, M. and Keshavarz, M. K., "Passive and electrochemical response of friction stir processed pure Titanium", J. Alloys Compd. 2017, 704, 499–508.
22. Banjare, P. N., Sahlot, P. and Arora, A., "An assisted heating tool design for FSW of thermoplastics", J. Mater. Process. Technol. 2017, 239, 83-91.
23. Eslami, S., Ramos, T., Tavares, P. J. and Moreira P. M. G. P., "Shoulder design developments for FSW lap joints of dissimilar polymers", J. Manuf. Process., 2015, 20(1), 15-23.
24. Simões, F. and Rodrigues, D. M., "Material flow and thermo-mechanical conditions during Friction Stir Welding of polymers: Literature

[Downloaded from idea.iust.ac.ir on 2024-07-29]

[DOI: 10.22068/ijmse.15.1.40]

review", experimental results and empirical analysis, Mater. Des. 2014, 59, 344-351.
25. Bozkurt, Y., "The optimization of friction stir welding process parameters to achieve maximum tensile strength in polyethylene sheets", Mater. Des. 2012, 35, 440-445.
26. Bagheri, A., Azdast, T., and Doniavi A., "An experimental study on mechanical properties of friction stir welded ABS sheets", Mater. Des. 2013, 43, 402-409.
27. Junior, W. S., Handge, U. A., Dos Santos, J. F., Abetz, V, and Amancio-Filho, S. T., "Feasibility study of friction spot welding of dissimilar single-lap joint between poly (methyl methacrylate) and poly (methyl methacrylate)-SiO_2 nanocomposite", Mater. Des. 2014, 64, 246-250.
28. Hoseinlaghab, S., Mirjavadi, S. S., Sadeghian, N., Jalili, I., Azarbarmas, M., and Besharati Givi, M. K., "Influences of welding parameters on the quality and creep properties of friction stir welded polyethylene plates", Mater. Des. 2015, 67, 369-378.
29. He, X, Gu, F, and Ball, A., A review of numerical analysis of friction stir welding, Prog. Mater. Sci. 2014, 65, 1-66.
30. Abbasi, M., Bagheri, B., and Keivani, R., "Thermal analysis of friction stir welding process and investigation into affective parameters using simulation", J. Mech. Sci. Technol. 2015, 29, 861-866.
31. Shi, L., and Wu, C. S., "Transient model of heat transfer and material flow at different stages of friction stir welding process", J. Manuf. Process., 2017, 25, 323-339.
32. Xiao, Y., Zhan, H., Gu, Y., and Li Q., "Modeling heat transfer during friction stir welding using a meshless particle method", J. Heat Mass Transfer, 2017, 104, 288-300.
33. Tang, J., and Shen, Y., "Numerical simulation and experimental investigation of friction stir lap welding between aluminum alloys AA2024 and AA7075", J. Alloys Compd. 2016, 666, 493-500.
34. Azarsa, E. and Mostafapour, A., "Experimental investigation on flexural behavior of friction stir welded high density polyethylene sheets", J. Manuf. Process., 2014, 16, 149-155.
35. Rezaee Hajideh, M., Farahani, M., Alavi, S. A. D., and Molla Ramezani, N., "Investigation on the effects of tool geometry on the microstructure and the mechanical properties of dissimilar friction stir welded polyethylene and polypropylene sheets", J. Manuf. Process., 2017, 26, 269-279.
36. Ansys Inc., ANSYS Mechanical APDL Theory Reference, 2013.
37. Mendes, N, Neto, P, Loureiro, A, and Moreira, A. P., "Machines and control systems for friction stir welding: A review", Mater. Des. 2016, 90, 256-265.
38. Mirjavadi, S., S., Alipour, M., Emamian, S., Kord, S., Hamouda, A. M. S., Koppad, P. G., and Keshavamurthy, R., "Influence of TiO2 nanoparticles incorporation to friction stir welded 5083 aluminum alloy on the microstructure", mechanical properties and wear resistance, J. Alloys Compd. 2017, 712, 795–803.
39. Liu, F. C., and Nelson, T. W., "In-situ grain structure and texture evolution during friction stir welding of austenite stainless steel", Mater. Des. 2017, 115, 467-478.

[Downloaded from idea.iust.ac.ir on 2024-07-29]

[DOI: 10.22068/ijmse.15.1.40]